Materials Chemistry and Physics 218 (2018) 189–195

Contents lists available at ScienceDirect

Materials Chemistry and Physics

journal homepage: www.elsevier.com/locate/matchemphys

Structural, thermal and nonlinear optical studies on novel organic cyclohexylammonium hydrogen adipate crystal

R. Gomathi, S. Madeswaran*

Advanced Materials Research Centre, Department of Physics, Vellore Institute of Technology, Vellore, 632014, India

HIGHLIGHTS

- CYHAD crystal possesses centro-symmetric space group P21/c.
- CYHAD has high transparency and low absorption which is essential for NLO applications.
- The CYHAD crystal thermally stable up to 168.01 °C and completely decomposed at 330 °C.
- Nonlinear optical studies revealed that the material is suitable for optoelectronic applications.

ARTICLE INFO

Keywords:
Crystal structure
Organic compounds
Nonlinear optic materials
Optical limiting
Dielectric materials

ABSTRACT

Single crystal of cyclohexylammonium hydrogen adipate (CYHAD) was grown from slow evaporation solution growth technique. The crystal structure and lattice parameters were determined by single crystal X-ray diffraction analysis. The material crystallized in monoclinic crystal system (P21/c). The FT-IR and CHN analysis were used to conform the functional group present in CYHAD. The material has high transparency with negligible absorption in the entire visible region and the optical band gap was found to be 4.90 eV. The PL spectrum shows the blue emission of CYHAD. The CYHAD crystal was stable up to 168.01 °C and the laser damage threshold of CYHAD was 9.74 GW/cm^2. Electrical properties were studied using LCR impedance analyzer. The third order nonlinear properties (n_2=-5.124 × 10^{-8} cm^2/W, β = 0.024 × 10^{-4} cm/W and χ^3 = 2.443 × 10^{-6} esu) were calculated using 532 nm diode pumped CW Nd:YAG Laser and optical limiting behavior endorse that the CYHAD material is favorable for optoelectronic applications.

1. Introduction

Organic materials have obtain recent attention due to their high nonlinear optical response, high thermal stability and chemical versatility for the applications of optical data storage, frequency doubling, wave guide fabrications and optical communications etc. [1–6]. The high value of nonlinear optical property can be attained by increasing π conjugation length and additionally introducing the electron donor and electron acceptor into the molecules [7]. Functional groups play an influencing role on the molecular assembly to form the larger single crystals in different dimensions. The hydrogen bond (X-H-A, where A is an acceptor molecule) has wide research interest due to its importance in organic chemistry, inorganic chemistry, bio chemistry, supramolecular chemistry and several other fields. Dimensionality of the supramolecular assembly, such as one-dimensional (1D), two-dimensional (2D) or three-dimensional (3-D) hydrogen-bonded assembly of molecules is a vital stepping stone to create efficient functional materials for different applications such as resonant cavity LEDs, resonant-cavity enhanced photo-detectors, vertical cavity surface emitting lasers, photonics and optoelectronics [40–43]. Carboxylic acid can form stronger hydrogen bond due to their stronger dipoles than other organic compounds such as amines, alcohols, phenols, aldehydes, ketones, esters, amides and isosteric compounds [10,11]. Cyclohexylamine is a strong alicyclic amine base which forms salts with all acids and the nitrogen atom present in cyclohexylamine is extremely reactive with organic compounds holding an active halogen atom and acid anhydrides [7–9]. Adipic acid was chosen as building block to construct organic crystal with cyclohexylamine base through hydrogen bond networks. In the recent years researchers are focusing a novel third order nonlinear optical material for photonic applications such as optical switching and optical limiting properties [12]. Most highly polarized nonlinear molecules have a tendency to pack centro

* Corresponding author.
E-mail address: madeswaran.s@vit.ac.in (S. Madeswaran).

https://doi.org/10.1016/j.matchemphys.2018.07.051
Received 25 January 2018; Received in revised form 4 July 2018; Accepted 22 July 2018
Available online 23 July 2018
0254-0584/

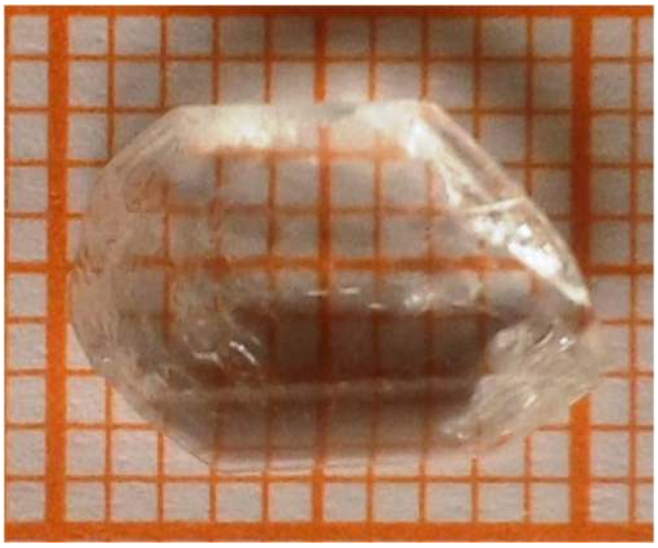

Fig. 1. As grown crystal of CYHAD.

symmetrically into a crystal lattice. The title compound with general formula (R-NH_3^+). (R'COO^-) has been investigated with cyclohexylamine and adipic acid. In the present work, we have analyzed the synthesis growth and characterization of CYHAD crystal.

2. Experimental work

All the reagents are purchased from Sigma Aldrich with 99% purification and used without further purification. To grow CYHAD single crystal (Fig. 1) cyclohexylamine (3.44 mL, 30 m mol) and adipic acid (4.3842 g, 30 m mol) in 20 mL of water was continuously stirred 12 h to attain homogeneous solution. The solution was filtered and kept in undisturbed place to evaporate slowly at room temperature and CYHAD crystal was harvested from the solution after a period of 17 days ($10 \times 7 \times 4\,mm^3$) using slow evaporation technique. The reaction scheme of the compound is given below.

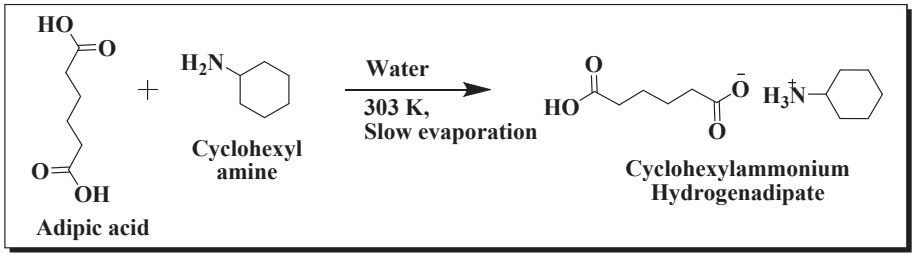

Table 1
Structural data of CYHAD crystal.

Formula	$C_{12}H_{23}NO_4$
Wavelength	0.71073
Crystal system, Space group	Monoclinic, P21/c
Formula weight	240.65
a	6.7231 (16) Å
b	20.423 (6) Å
c	10.384 (3) Å
α	90 °
β	96.024 (9) °
γ	90 °
V	1417.9 (7) $Å^3$
T/K	293 (2)
Z	4
Density	1.127 g/cm^2
Goodness of fit	1.025
Extinction coefficient	0.038 (9)
R_(all)	0.1321
R_(gt)	0.0862
wR_ref	0.2983
wR_gt	0.2460
Δρmax	0.575
Δρmin	−0.329
(Δ/σ)max	0.072
CCDC No	1551082

3. Results and discussion

3.1. Single crystal X-ray diffraction analysis

The structure and lattice parameters of CYHAD were determined using single crystal X ray diffractometer (ENRAF BRUKER NONIUS CAD4 with MoKα radiation). The dimension of 0.20 × 0.25 × 0.30 mm (CYHAD) is used and the total reflections (2721) were collected at 293 (2) K in the range of 2.21 °–23.35° with the limiting indices range (h,k,l) −8→8, −24→24, −12→12 respectively. The structure of the crystal was solved by direct method and refined by full matrix least-square method using SHELXS-14 program. The CYHAD crystal belongs to monoclinic crystal system with centro-symmetric space group (P21/c) and the estimated cell parameters are tabulated in Table 1. The asymmetric unit of the title material consists of one cyclohexylammonium cation and one hydrogen adipate anion and the crystal structure shows that the cyclic amine contains a positively charged protonated amino group and a negatively charged deprotonated carboxyl group. The cyclohexylammonium cation interacts through N-H-O hydrogen bond to neighboring carboxylate anion. It is very interesting to noted that the C-O bond length recorded for hydrogen adipate is very similar (C8-O3 = 1.205 Å, C8-O4 = 1.299 Å, C13-01 = 1.235 (4) Å and C13-O2 = 1.261 (4) Å) [45]. The nitrogen atom bound to carbon was optimized with N1-C1 = 1.483 (5) Å. The H atoms bound to N atom were geometrically optimized with N-H (N1-H1 = 0.92 Å, N1-H2 = 0.73 Å and N1-H3 = 0.86 Å). Similarly the hydrogen atom in CYHAD was also geometrically optimized with O-H (0.82 Å) which confirms the formation of cyclohexylammonium hydrogen adipate crystal. In CYHAD the hydrogen adipate anion alone form a one dimensional hydrogen bonded chain running parallel to (001) direction. The O4-H4···O3 hydrogen bond links (symmetry code: x,-y+1, z+1/2) the anions by glide plane perpendicular to (0,1,0) and the glide component is (0,0,1/2) ending with an anionic structure [44–46]. Fig. 2 shows the ORTEP diagram and packing diagram of CYHAD. From Fig. 2 b the blue color represented the intermolecular interaction between N-H-O atoms. The bond length and bond angles are presented in Table 2.

Symmetry transformations used to generate equivalent atoms:

'x, y, z'; '-x, y+1/2, -z+1/2'; '-x, -y, -z'; 'x, -y-1/2, z-1/2'

3.2. FT-IR and CHN analysis

FT-IR spectrum of CYHAD recorded in the range of 400–4000 cm^{-1} using SHMADZU IR Affinity-1s spectrometer with KBr pellet technique. Fig. 3 shows the FT-IR spectrum of CYHAD. The bands observed at

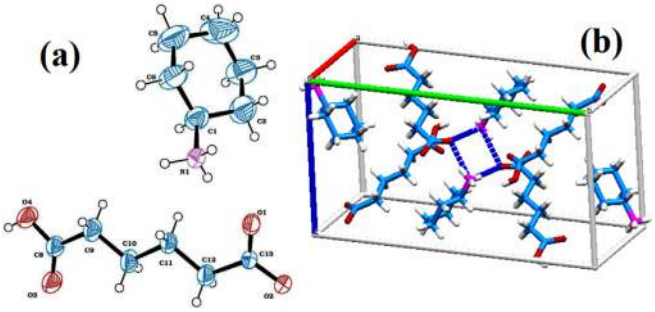

Fig. 2. a. ORTEP diagram and b. Packing diagram of CYHAD.

Table 2
Bond length and bond angles of CYHAD crystal.

Atoms	Length	Atoms	Angels
C1-C2	1.449 (7)	C2-C1-C6	113.7 (4)
C1-C6	1.461 (7)	C2-C1-N1	111.1 (4)
C1-N1	1.483 (5)	C6-C1-N1	110.8 (4)
C2-C3	1.536 (9)	C1-C2-C3	110.5 (5)
C3-C4	1.475 (9)	C4-C3-C2	110.1 (6)
C4-C5	1.441 (9)	C5-C4-C3	114.4 (6)
C5-C6	1.556 (8)	C4-C5-C6	109.4 (6)
C8-O3	1.205 (5)	C1-C6-C5	111.3 (5)
C8-O4	1.299 (5)	O3-C8-O4	123.1 (3)
C8-C9	1.496 (5)	O3-C8-C9	124.7 (3)
C9-C10	1.495 (5)	O4-C8-C9	112.2 (3)
C10-C11	1.512 (5)	C8-C9-C10	114.5 (3)
C11-C12	1.497 (5)	C9-C10-C11	113.1 (3)
C12-C13	1.504 (5)	C12-C11-C10	112.8 (3)
C13-O1	1.235 (4)	C11-C12-C13	116.8 (3)
C13-O2	1.261 (4)	O1-C13-O2	122.9 (3)
N1-H1	0.92 (4)	O1-C13-C12	120.8 (3)
N1-H2	0.73 (4)	O2-C13-C12	116.2 (3)
N1-H3	0.86 (4)	H1-C1-N1	106.9
O4-H4	0.82 (4)	C8-O4-H4	109.5

2937, 2540 cm^{-1} and 2848 cm^{-1} represents the NH_3^+ plane in symmetric stretching and CH symmetric stretching respectively [13]. The peak at 1716 cm^{-1} indicates C=O stretching and the peak at 1294 represents C-O stretching of the acid. The NH_3^+ symmetric deformation identified at 1537 cm^{-1} [14]. The peaks at 707 cm^{-1} and 513 cm^{-1} assigned to COOH rocking and C-C=O wagging respectively. The C-N stretching and COO^- stretching was identified at 1406 cm^{-1} and 1624 cm^{-1} respectively. The bending and wagging vibrations of CH group represented at 1234 cm^{-1} and 1182 cm^{-1} respectively. The peak

Table 3
Vibrational assignments of CYHAD.

Wave number (cm^{-1})	Assignment
2937	NH_3^+ in plane symmetric stretching
2848	CH symmetric stretching
2540	NH_3^+ symmetric stretching
1716	C=O stretching
1624	COO^- stretching
1537	NH_3^+ symmetric deformation
1406	C-N stretching
1294	C-O stretching vibration
1234, 1182	CH bending and wagging vibration
896	NH wagging
707	COOH rocking
513	C-C=O wagging

Table 4
CHN analysis data of CYHAD.

CYHAD	C (%)	H (%)	N (%)
Theoretical	5.71	58.75	9.45
Experimental	5.57	58.29	9.308

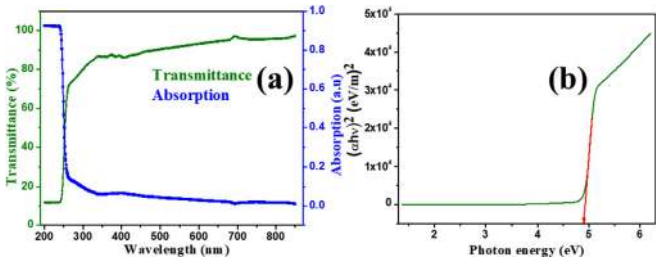

Fig. 4. a. UV–Vis–NIR spectrum and c. Tauc's plot of CYHAD.

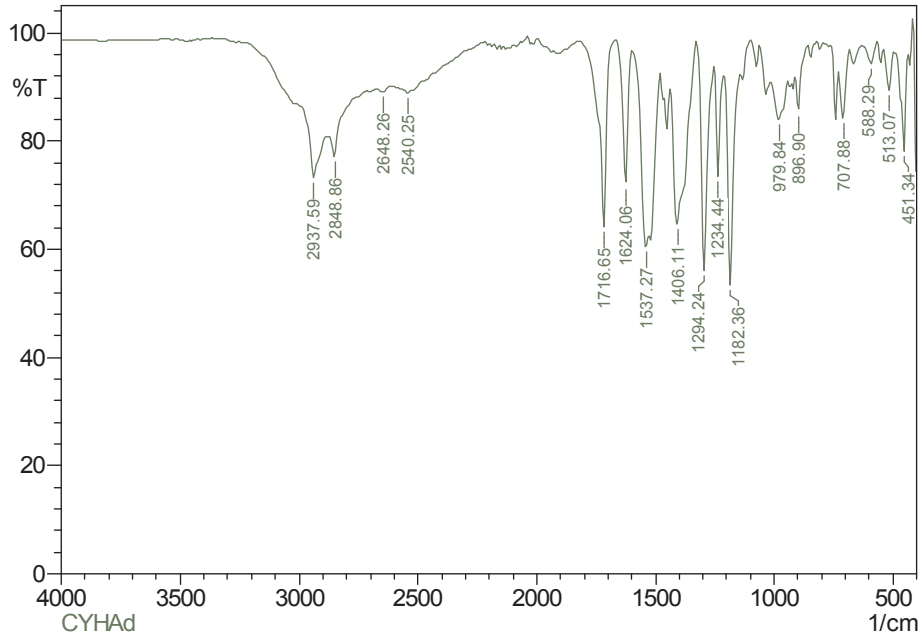

Fig. 3. FT-IR spectrum of CYHAD crystal.

at 896 cm^{-1} and 588 cm^{-1} were due to the N-H wagging and NH_3^+ torsional oscillation [39]. This confirms the CYHAD compound formation and the corresponding functional groups are tabulated in Table 3.

The CHN elemental analysis of CYHAD was carried out using Perkin-Elmer Series II 2400 CHNS/O Elemental Analyzer and the corresponding data are given in Table 4. The data shows the good agreement with the theoretical value within the limits of permissible error and confirms the formation of CYHAD.

3.3. UV–Vis–NIR analysis

The linear optical properties (transmittance, reflectance and refractive index) of CYHAD (1 mm thickness) were calculated using JUASCO-V-650 in the range of 200–850 nm. Fig. 4 a shows the transmittance and absorption spectrum of CYHAD and the cut off wavelength of CYHAD is 252 nm. It is due to the n-π^* electronic transition [38]. The transparency of CYHAD is ≈ 90% and the absorption is negligible in the entire visible region. This is the essential property for nonlinear optical applications. The absorption coefficient (α) and optical band gap were calculated using the following relation [31,32],

$$\alpha = \frac{2.3026\log\left(1/T\right)}{t} \quad (1)$$

$$\alpha h\vartheta = A(h\vartheta - E_g)^{\frac{1}{2}} \quad (2)$$

where, t is the thickness of the sample, A is a constant, h is plank constant, ϑ is the frequency of incident photons, E_g is optical band gap and T is transmittance of the sample. The band gap was calculated using Tauc's plot and it is found to be 4.90 eV (Fig. 4 b). The extinction coefficient (K) explains the quantity of absorption when an electromagnetic wave propagate through the material and it has direct relation with the absorption of the material. The extinction coefficient, reflectance and refractive index of CYHAD was calculated using the relations [33–35].

$$K = \frac{\alpha\lambda}{4\pi} \quad (3)$$

$$R = \frac{\exp(-\alpha t) \pm \sqrt{\exp(-\alpha t)T - \exp(-3\alpha t)T + \exp(-2\alpha t)T^2}}{\exp(-\alpha t) + \exp(-2\alpha t)T} \quad (4)$$

$$n = \frac{-(R-1) \pm 2\sqrt{R}}{(R-1)} \quad (5)$$

From Fig. 5 a, and b, it is clear that the extinction coefficient, reflectance and refractive index are strongly depends on photon energy and the low value of K indicates the less absorption of the material which is suitable for device applications in computing and information processing [34]. The refractive index at 850 nm is 1.7842.

3.4. Thermal studies

The thermal stability of the sample was determined using thermogravimetric analysis (TGA) and differential scanning colorimetry (DSC). The TGA-DSC analyses of CYHAD were carried out at a heating rate of 20 °C min^{-1} in nitrogen atmosphere in the range of 30–400 °C. The total amount of salt used for the analysis was 5.2510 mg. From Fig. 6 we have concluded that there is a single stage consecutive weight loss (99.33%) occurred at about 168–330 °C. The absence of weight loss near 100 °C represented that there is no water molecule present in CYHAD and the decomposition takes place in a single stage into volatile gaseous products such as CO_2 NH_3 and CO [36]. The DSC curve indicates similar changes as shown in TGA curve. The sharp endothermic peak at 168.01 °C indicates the melting point of CYHAD and this value is comparable with other cyclohexylammonium carboxylate crystals [37,38] like CYHPH (146 °C) and CYHAC (161 °C). As it is stable up to 168.01 °C, it is suitable candidate for nonlinear optical applications up-to this range [15]. The specific heat capacity of CYHAD (265.12 J/g/K) was determined from DSC analysis using the formula, $\frac{dH}{dT} = mC_p\frac{dT}{dt}$. Here, $\frac{dH}{dT}$ is heat flow J/g), m is sample mass (g), C_p is specific heat capacity and $\frac{dT}{dt}$ is program rate (K/s).

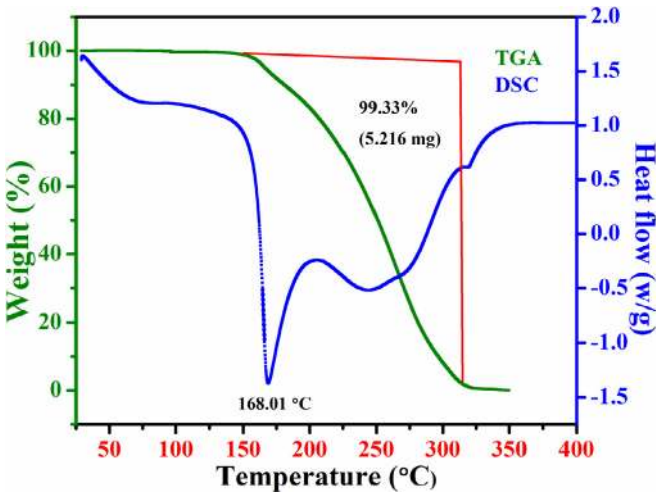

Fig. 6. TGA-DSC spectrum CYHAD.

3.5. Dielectric studies

Dielectric properties of CYHAD were analyzed using LCR impedance analyzer in the range of 100 Hz–5 MHz at various temperatures

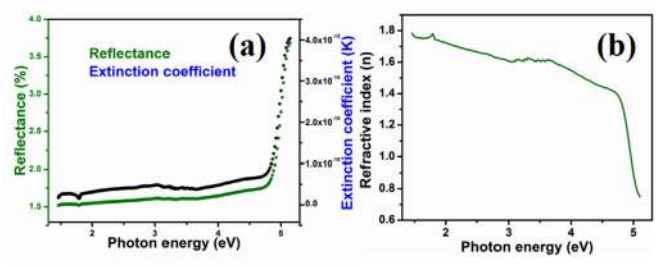

Fig. 5. a Variation of extinction coefficient and reflectance with photon energy and b. Variation of refractive index with photon energy.

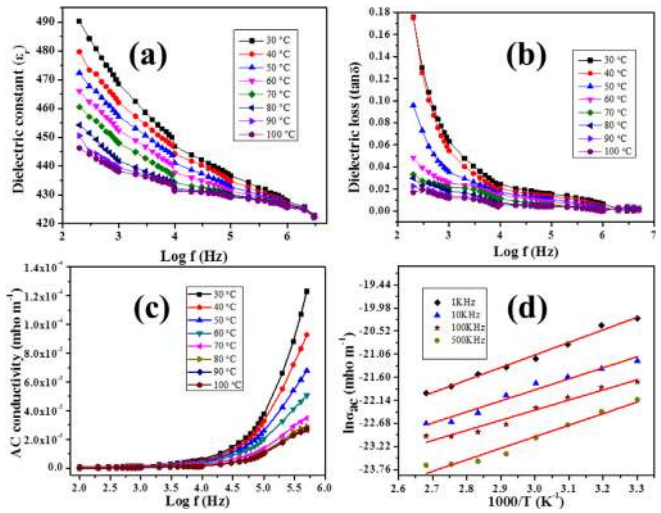

Fig. 7. a. Dielectric constant, b. Dielectric loss of CYHAD crystal, c. AC conductivity and d. 1000/T Vs lnσ_{ac} of CYHAD crystal.

(30 °C–100 °C). A well transparent crystal with area of 22 mm^2 and thickness of 1.37 mm was coated using silver paste on both side and placed between two nickel electrodes, which form a parallel plate capacitor. Fig. 7a and b shows similar variation that is dielectric constant (ε_r) and loss (tanδ) were decreasing with increase in frequency. The high value of ε_r and tanδ at low frequency is due to the presence of four types of polarization (electronic, ionic, orientation and space charge polarization) present in the material [16]. Hence, the high frequency region where we have less dielectric permittivity and low loss of CYHAD is suitable for the applications of electro-optic modulator, photonics, microelectronics and field detector device [17,18].

3.6. AC conductivity study

The AC conductivity of grown crystal was calculated using the relation [28],

$$\sigma_{ac} = 2\pi f \varepsilon_r \varepsilon_0 \tan\delta \quad (6)$$

here, ε_r is relative dielectric constant, ε_0 is vacuum dielectric constant, f is frequency of applied electric field and $tan\delta$ is loss tangent. Fig. 7 c shows the variation of alternating current conductivity with frequency at different temperatures (30–100 °C). At low frequencies, the accumulation of charge occurs and drops in conductivity. In the plateau region (intermediate frequency region), the conductivity is frequency independent and it is obtained due to the transport of mobile ions in response to the electric field. At high frequency region, conductivity increases with frequency which is due to the long range movement of charge carriers [29]. Fig. 7 d represents the plot between ln σ_{ac} and 1000/T. The activation energy was calculated using the relation [30], $\sigma_{ac} = \sigma_0 \exp\left(\frac{-E_a}{KT}\right)$ where, σ_0 is constant, E_a is activation energy, K is Boltzmann constant (1.380×10^{-23}) and T is the absolute temperature. The activation energy was calculated to be 0.25 eV, 0.22 eV, 0.20 eV and 0.23 eV at 1 KHz, 10 KHz, 100 KHz and 500 KHz respectively.

3.7. Photoluminescence spectroscopy

PL (Photoluminescence) analysis is a reliable and non-destructive tool to understand the luminescence property of the material. The PL emission spectrum of CYHAD was recorded in the range between 430 and 750 nm using Cary Eclips fluorescence spectrometer with an input excitation wavelength of 235 nm and the corresponding emission (λ_{max}) was observed at 474 nm which is due to the n-π* transition between the donor primary amine and acceptor COOH group [31] depicting blue emission. Further the weaker emission in the higher wavelength region

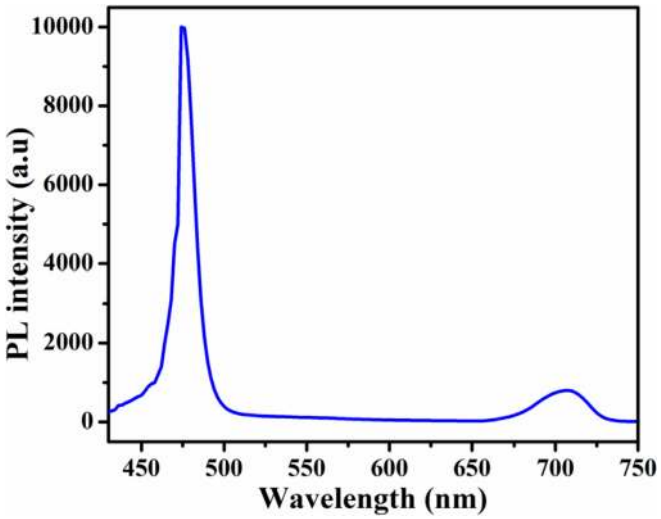

Fig. 8. PL spectrum of CYHAD.

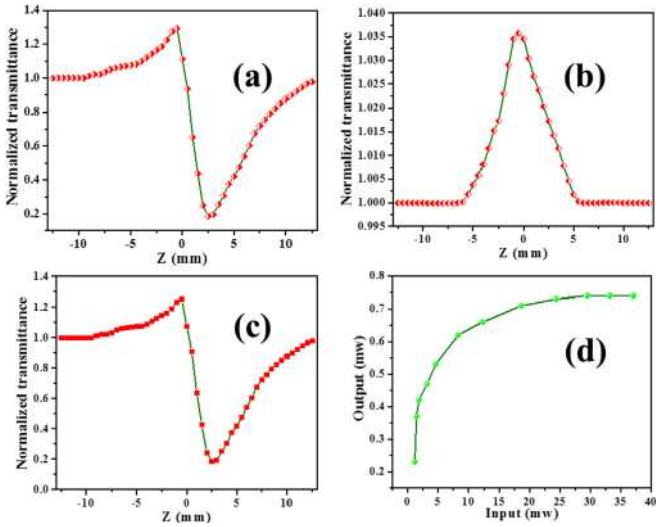

Fig. 9. a. Closed aperture, b. Open aperture, c. Ratio of closed to open aperture curve and d. Optical limiting spectrum.

affirms the large hydrogen bond associated in the crystal lattice [24]. The PL signal mainly depends on density of photo-excited electrons, the incident beam intensity, wavelength and also change with excitation energy [50]. From Fig. 8, it is shown that the emission peak largely shifts towards the higher wavelength region. It can be explained that the excitation states controls the photo-excited electrons and holes density and each electron-hole pair recombination mechanism was depends on carrier density [51]. In the case of 235 nm (excitation wavelength), the emission peak was identified at 478 nm. Hence it can be considered for optoelectronic device application particularly in the blue emission regime.

3.8. Nonlinear optical studies

The nonlinear optical properties of CYHAD (1 mm thickness) were characterized by Z - scan technique using 532 nm diode pumped CW Nd:YAG Laser (Coherent CompassTM215M − 50 and focal length f = 3.5 cm). The change in transmittance with sample position were shown in Fig. 9a, and b which indicates the self-defocusing and saturable absorption present in the compound and Fig. 9c represents the ratio of closed to open aperture spectrum. On-axis phase shift (ΔΦ) can be calculated from the difference between peak and valley transmittance using the following equation [19],

$$\Delta T_{P-V} = 0.406(1 - S)^{0.25}|\Delta\Phi| \quad (7)$$

here, S is aperture linear transmittance which is obtained from the relation S = 1-exp ($-2r_a^2/\omega_a^2$), where r_a is radius of the aperture and ω_a is the beam radius at the aperture. The nonlinear absorption coefficient (β) and third order nonlinear refractive index related to ΔΦ are given by Refs. [20,21],

$$\beta = \frac{2\sqrt{2}\Delta T}{I_0 L_{eff}} \quad (8)$$

$$n_2 = \frac{\Delta\Phi}{k I_0 L_{eff}} \quad (9)$$

where, ΔT is the valley value at the open aperture curve, L_{eff} is an effective thickness of the crystal ($L_{eff} = \frac{1-\exp(-\alpha L)}{\alpha}$) and k is the wave number ($k = 2\pi/\lambda$). I_0 is the intensity of the laser beam, α is linear absorption and L is thickness of the sample.

The third order nonlinear optical susceptibility (χ^3) was calculated using [22],

Table 5
Comparison of M.P, χ^3, LDT of CYHAD with other organic crystal.

Crystal	Melting point (°C)	χ^3 (esu)	LDT (GW/cm^2)	Reference
KDP	213	4.02×10^{-14}	0.20	[24,25]
Benzimidazole (by SEST)	–	–	1.71	[25]
Benzimidazole (by VBT)	–	–	2.86	
QN	174	-4.07×10^{-12}	15.54	[26]
VMST	–	9.6963×10^{-12}	1.59	[27]
P2HP	–	5.8032×10^{-6}	3.22	
CYHAD	168.01	2.443×10^{-6}	9.74	Present

$$|\chi^{(3)}| = [(R_e(\chi^{(3)}))^2 + (I_m(\chi^{(3)}))^2]^{1/2} \quad (10)$$

The real and imaginary part of third order susceptibility were found from the formula,

$$R_e(\chi^{(3)})esu = \frac{10^{-4}\varepsilon_0 C^2 n_0^2 n_2}{\pi}\ \mathrm{cm^2W^{-1}} \quad (11)$$

$$I_m(\chi^{(3)})esu = \frac{10^{-2}\varepsilon_0 C^2 n_0^2 \lambda\beta}{4\pi^2}\mathrm{cm^2W^{-1}} \quad (12)$$

where, ε_0 is the vacuum permittivity ($8.854 \times 10^{-12}\ Fm^{-1}$), c is the velocity of light and $n_\circ$ (3.79) is the linear refractive index of the crystal. The values of n_2, β and χ^3 are found to be -5.124×10^{-8} cm^2/W, 0.024×10^{-4} cm/W and 2.443×10^{-6} esu respectively. Optical limiting (OL) properties of materials have important application because that consumes potentially damaging light of intense irradiation for the protection of photo sensors and human eyes [23]. OL behavior was tested using Nd:YAG laser source at 532 nm. The sample was employed at valley position of Z scan pattern and the corresponding limiting trace was measured (Fig. 9d). It is clear that two typical regions were observed, in the first regime the output power varied linearly with the input power according to beer- Lambert law and it goes through a plateau at second region. The optical limiting threshold and the corresponding output clamping were found to be 24.3 mW and 0.73 mW respectively.

3.9. Laser damage threshold studies

Nonlinear optical device involves the exposure of the NLO material to high power laser source. Hence, the material should tolerate high laser intensity for the laser power related applications. In order to measure the optical surface damage tolorence of CYHAD we have analyzed the laser damaged threshold measurement (LDT). LDT measurement plays a major role in improving the quality of military optics. A flat surface of CYHAD crystal with 3.22 mm thickness was used to perform LDT measurement using Q-switched high energy Nd:YAG Laser (QUANTA RAY model) at 1064 nm with the focal length of biconvex lens 15 cm. The energy range was 1.5 mJ–3 J and the repetition rate was 10 Hz. The energy density (I) was calculated using the relation [47],

$$I = \frac{E}{\tau A} \quad (13)$$

where, E is input laser beam energy density (mJ), τ is pulse width (6 ns) and A is the area of the circular spot (mm). Hence the incident intensity can be increased either by focusing the power into smaller cross-sectional area or by increasing the laser beam power. There is a limit to increase the laser strength as it may lead to the damage of the crystal called damage threshold. Generally two main mechanism (thermal absorption and electron avalanche) causes laser damage in materials. Thermal absorption arises from the deposition of laser energy in the material. Electron avalanche arises due to the energy delivered at a high intensity or the electric field density is high enough to strip electrons from the lattice [52]. The avalanche ionization also takes place when the pulse length is short enough and the avalanche threshold to be below the thermal threshold (thermal absorption is low enough). Laser damage may be produced by single mechanism or both these mechanisms in concert. When a laser beam passes through the material, absorption can occur which produce heat inside the material leads to the appearance of inhomogeneous wave mismatch and temperature instability, result in the generation of cracks. The thermal absorption observed during radiation of continuous wave, long pulse lengths, and high pulse-repetition-frequency pulse trains. Here the damage mechanism arising due to the thermal absorption. If the specific heat of the crystal high (265.12 J/g/K), then the temperature gradient will be small which will minimize the formation of cracks in the crystal [49]. The damage threshold depends on the laser parameters such as wavelength, pulse duration, transverse and longitudinal mode structure, energy, beam size and location of beam [48]. The calculated LDT, melting point (M.P) and χ^3 were compared with other known materials and are tabulated in Table 5.

4. Conclusion

In summary, a novel organic monoclinic (P21/c) CYHAD crystal with dimensions of $10 \times 7 \times 4\ mm^3$ was grown by slow evaporation technique. The functional group was confirmed using FT-IR analysis and CHN analysis. The cut off wavelength and band gap energy were found to be 252 nm and 4.90 eV respectively. The thermal analysis shows the melting point (168.01 °C) of CYHAD crystal and the PL spectrum shows that the material has blue emission. The low value of dielectric constant and loss suggest that the material is suitable for photonic and microelectronic device applications. The activation energy at 1 KHz, 10 KHz, 100 KHZ and 500 KHz are found to be 0.25 eV, 0.22 eV, 0.20 eV and 0.23 eV respectively. The laser damage threshold study reveals that the material has high laser power tolerance, suitable in high power frequency applications. Z-scan analysis and optical limiting behavior reveals that the CYHAD possess large nonlinear response. Hence it may be concluded that the material is favorable candidate for photonic, microelectronic and optical limiting applications.

Acknowledgements

The authors acknowledge Vellore Institute of Technology, Vellore for providing excellent research facility and one of the author R.G thanks to VIT management for providing Research Associateship.

References

[1] M.L. Schilling, V.L. Colvin, L. Dhar, A.L. Harris, F.C. Schilling, H.E. Katz, T. Wysocki, A. Hale, L.L. Blyler, C. Boyd, Chem. Mater. 11 (1999) 247–254.
[2] C. Zhang, Y.S. Zhao, J. Yao, Phys. Chem. Chem. Phys. 13 (2011) 9060–9073.
[3] A.J.C. Kuehne, M.C. Gather, Chem. Rev. 116 (2016) 12823–12864.
[4] H. Dong, H. Zhu, Q. Meng, X. Gong, W. Hu, Chem. Soc. Rev. 41 (2012) 1754–1808.
[5] A. Ségerie, F. Castet, M.B. Kanoun, A. Plaquet, V. Liégeois, B. Champagne, Chem. Mater. 23 (2011) 3993–4001.
[6] H.S. Nagaraja, V. Upadhyaya, P.M. Rao, P.S. Aithal, A.P. Bhat, J. Cryst. Growth 193 (1998) 674–678.
[7] A. Lemmerer, Cryst. Growth Des. 11 (2011) 583–593.
[8] J.A. Odendal, J.C. Bruce, K.R. Koch, D.A. Haynes, CrystEngComm 12 (2010) 2398–2408.
[9] Y.Z. Tang, Y.M. Yu, J.B. Xiong, Y.H. Tan, H.R. Wen, J. Am. Chem. Soc. 137 (2015) 13345–13351.
[10] D. Balasubramanian, P. Murugakoothan, R. Jayavel, J. Cryst. Growth 312 (2010) 1855–1859.
[11] V. Subhashini, S. Ponnusamy, C. Muthamizhchelvan, J. Cryst. Growth 363 (2013) 211–219.
[12] H.S. Nalwa, Adv. Mater. 5 (1993) 341–358.
[13] R. Padmavathy, N. Karthikeyan, D. Sathya, R. Jagan, R.M. Kumar, K. Sivakumar, RSC Adv. 6 (2016) 68468–68484.
[14] J.E.M. Theras, D. Kalaivani, D. Jayaraman, V. Joseph, J. Cryst. Growth 427 (2015) 29–35.
[15] J. Mary Linet, S. Jerome Das, Mater. Chem. Phys. 126 (2011) 886–890.
[16] T. Suthan, N.P. Rajesh, C.K. Mahadevan, G. Bhagavannarayana, Mater. Chem. Phys.

129 (2011) 433–438.
[17] L.R. Dalton, J. Phys. Condens. Matter 15 (2003) 897–934.
[18] M. Anis, S.S. Hussaini, M.D. Shirsat, G.G. Muley, Mater. Sci. Poland 34 (2016) 548–554.
[19] R. Thirumurugan, K. Anitha, Mater. Lett. 206 (2017) 30–33.
[20] X.Q. Wanga, Q. Ren, J. Sun, H.L. Fan, T.B. Li, X.T. Liu, G.H. Zhang, L.Y. Zhu, D. Xu, J. Cryst. Growth 324 (2011) 124–129.
[21] I.P. Bincy, R. Gopalakrishnan, J. Cryst. Growth 402 (2014) 22–31.
[22] P. Rekha, G. Peramaiyan, M. NizamMohideen, R.M. Kumar, R. Kanagadurai, J. Cryst. Growth 441 (2016) 18–25.
[23] A. Vijayalakshmi, B. Vidyavathy, G. Vinitha, J. Cryst. Growth 448 (2016) 82–88.
[24] N. Vijayan, G. Bhagavannarayana, G.C. Budakoti, B. Kumar, V. Upadhyaya, S. Das, Mater. Lett. 62 (2008) 1252–1254.
[25] N. Vijayan, G. Bhagavannarayana, R. Ramesh Babu, R.K.K. Maurya, P. Ramasamy, Cryst. Growth Des. 6 (2006) 1542–1546.
[26] J. Mohana, G. Ahila, M.D. Bharathi, G. Anbalagan, J. Cryst. Growth 450 (2016) 181–189.
[27] I.M. Zahid, C.A. Kumar, A. Malarkodi, K.J. Wilson, R.M. Kumar, Mater. Lett. 209 (2017) 167–170.
[28] P. Singh, M. Hasmuddin, M. Shakir, N. Vijayan, M.M. Abdullah, V. Ganesh, M.A. Wahab, Mater. Chem. Phys. 142 (2013) 154–164.
[29] T. Badapanda, R.K. Harichandan, S.S. Nayak, A. Mishra, S. Anwar, P. Appl. of Ceramics 8 (2014) 145–153.
[30] B. Uma, K.S. Murugesan, S. Krishnan, R. Jayavel, B.M. Boaz, Mater. Chem. Phys. 142 (2013) 659–666.
[31] S. Chandran, R. Paulraj, P. Ramasamy, Opt. Mater. 52 (2016) 49–55.
[32] P. Karthiga Devi, K. Venkatachalam, M. Poonkothai, J. Mol. Struct. 1119 (2016) 462–47.
[33] M. Shkir, S. AlFaify, H. Abbas, G. Bhagavannarayana, Mater. Chem. Phys. 155 (2015) 36–46.
[34] V. Sangeetha, K. Gayathri, P. Krishnan, N. Sivakumar, N. Kanagathara, G. Anbalagan, J. Cryst. Growth 389 (2014) 30–38.
[35] K. Thukral, N. Vijayan, M. Vij, C.M. Nagaraja, V. Jayaramakrishnan, M.S. Jayalakshmy, R. Kant, Mater. Chem. Phys. 194 (2017) 90–96.
[36] P. Prabukanthan, R. Lakshmi, G. Harichandran, C.S. Kumar, J. Mol. Struct. 1156 (2018) 62–73.
[37] R. Gomathi, S. Madeswaran, D. Rajan Babu, J. Mater. Sci. Mater. Electron. 28 (2017) 11374.
[38] R. Gomathi, S. Madeswaran, D. Rajan Babu, G. Aravindan, Mater. Lett. 209 (2017) 240.
[39] M. Saravanana, A. Senthil, S.A. Rajasekar, Optik 127 (2016) 1372–1377.
[40] J. Muszalski, Acta Phys. Pol., A 114 (2008) 983–999.
[41] K.E. Maly, T. Maris, J.D. Wuest, Cryst. Eng. Commun. 8 (2006) 33–35.
[42] D. Kong, Abraham Clearfield, Cryst. Growth Des. 5 (2005) 1767–1773.
[43] C.Y. Liu, V. Lynch, A.J. Bard, Chem. Mater. 9 (1997) 943–949.
[44] R. Jagan, K. Sivakumar, Acta Crystallogr. C67 (2011) o373–o377.
[45] M. Sarr, A. Diasse-Sarr, L. Diop, L. Plasseraud, H. Cattey, Acta Crystallogr. E71 (2015) 899–901.
[46] A. Lemmerer, S.A. Bourne, M.A. Fernandes, CrystEngComm 10 (2008) 1605–1612.
[47] N. Rani, N. Vijayan, B. Riscob, S.K. Jat, A. Krishna, S. Das, G. Bhagavannarayana, B. Rathi, M.A. Wahab, CrystEngComm 15 (2013) 2127–2132.
[48] G.C. Bhar, A.K. Chaudhary, P. Kumbhakar, Appl. Surf. Sci. 161 (2000) 155–162.
[49] A. Krishna, N. Vijayan, S. Gupta, K. Thukral, V. Jayaramakrishnan, B. Singh, J. Philip, S. Das, K.K. Maurya, G. Bhagavannarayana, RSC Adv. 4 (2014) 56188–56199.
[50] T.H. Gfroerer, Photoluminescence in analysis of surfaces and interfaces, in: R.A. Meyers (Ed.), Encyclopedia of Analytical Chemistry, John Wiley and Sons Ltd., Chichester, 2000, pp. 9209–9231.
[51] N.S. Sowmya, S. Sampathkrishnan, Y. Vidyalakshmi, S. Sudhahar, R.M. Kumar, Spectrochim. Acta Mol. Biomol. Spectrosc. 145 (2015) 333–339.
[52] J. Yu, X. Xiang, S. He, X. Yuan, W. Zheng, H. Lü, X. Zu, Adv. Condens. Matter Phys. (2014) 1–10, https://doi.org/10.1155/2014/364627.